A role for *Toxoplasma gondii* chloroquine resistance transporter in bradyzoite viability and digestive vacuole maintenance

Geetha Kannan[a], Manlio Di Cristina[b], Aric J. Schultz[a], My-Hang Huynh[a], Fengrong Wang[a], Tracey L. Schultz[a,*], Matteo Lunghi[b,**], Isabelle Coppens[c], Vern B. Carruthers[1,#]

[a]Department of Microbiology and Immunology, University of Michigan Medical School, Ann Arbor, MI 48109, USA

[b]Department of Chemistry, Biology and Biotechnology, University of Perugia, Perugia 06122, Italy

[c]Department of Molecular Microbiology and Immunology, The Johns Hopkins University Bloomberg School of Public Health, Baltimore, MD 21205, USA

Running head: Role of TgCRT in chronic *Toxoplasma* infection

[#]Address correspondence to: Vern B. Carruthers, vcarruth@umich.edu

*Present address: Biosciences Center, National Renewable Energy Laboratory, Golden, CO, USA

**Present address: Department of Microbiology and Molecular Medicine, CMU, University of Geneva, 1 Rue Michel-Servet CH-1211 Geneva 4, Switzerland

ABSTRACT

Toxoplasma gondii is a ubiquitous pathogen that can cause encephalitis, congenital defects, and ocular disease. *T. gondii* has also been implicated as a risk factor for mental illness in humans. The parasite persists in the brain as slow growing bradyzoites contained within intracellular cysts. No treatments exist to eliminate this form of parasite. Although proteolytic degradation within the parasite lysosomal-like vacuolar compartment (VAC) is critical for bradyzoite viability, whether other aspects of the VAC are important for parasite persistence remains unknown. An ortholog of *Plasmodium falciparum* CRT has previously been identified in *T. gondii* (TgCRT). To interrogate the function of TgCRT in chronic stage bradyzoites and its role in persistence, we knocked out TgCRT in a cystogenic strain and assessed VAC size, VAC digestion of host- derived proteins and parasite autophagosomes, and viability of *in vitro* and *in vivo* bradyzoites. We found that whereas parasites deficient in TgCRT exhibit normal digestion within the VAC, they display a markedly distended VAC and their viability is compromised both *in vitro* and *in vivo*. Interestingly, impairing VAC proteolysis in TgCRT deficient bradyzoites restored VAC size, consistent with a role for TgCRT as a transporter of products of digestion from the VAC. In conjunction with earlier studies, our current findings suggest a functional link between TgCRT and VAC proteolysis. This work provides further evidence of a crucial role for the VAC in bradyzoite persistence and a new potential VAC target to abate chronic *Toxoplasma* infection.

IMPORTANCE

Individuals chronically infected with the intracellular parasite *Toxoplasma gondii* are at risk of experiencing reactivated disease that can result in progressive loss of vision. No

effective treatments exist for chronic toxoplasmosis due in part to a poor understanding of the biology underlying chronic infection and a lack of well validated potential targets. Here we show that a *T. gondii* transporter is functionally linked to protein digestion within the parasite lysosome-like organelle and that this transporter is necessary to sustain chronic infection in culture and in experimentally infected mice. Ablating the transporter results in severe bloating of the lysosome-like organelle. Together with earlier work, this study suggests the parasite's lysosome-like organelle is vital for parasite survival, thus rendering it a potential target for diminishing infection and reducing the risk of reactivated disease.

INTRODUCTION

Toxoplasma gondii (*T. gondii*) is an opportunistic pathogen that causes encephalitis or debilitating ocular and congenital diseases in humans (1-4). It has also been implicated as a risk factor for schizophrenia and other major mental illnesses (5-8). The parasite progresses through two major life stages during infection of its intermediate hosts: the acute stage characterized by actively replicating tachyzoites and the chronic stage featuring slow growing bradyzoite cysts that persist in muscle and brain tissue (9). While drugs exist against acute stage tachyzoites, currently no treatments are available to combat the chronic stage bradyzoite cysts. The development of new interventions for limiting disease from chronic infection is hindered by a lack of well-validated potential targets and understanding of the biology of *T. gondii* bradyzoites.

One avenue toward this goal is to define the contributions of proteins associated with the parasite Plant-Like Vacuole (PLV)/Vacuolar Compartment (VAC, used hereafter). The *T. gondii* VAC is a lysosome-like organelle that contains a variety of proteases, including

73 those of the cathepsin family (10, 11). It was previously shown that *T. gondii* cathepsin
74 protease L (TgCPL) localizes to the lumen of the VAC where it aids in the digestion of
75 ingested host-derived proteins and parasite autophagosomes (11-13). Diminishing the
76 digestive function of the VAC by either genetic ablation of TgCPL or chemical inhibition of
77 TgCPL with morpholinurea-leucine-homophenylalanine-vinyl phenyl sulphone (LHVS)
78 revealed an critical role for the VAC in parasite viability, particularly in the bradyzoite stage
79 (11, 13, 14).
80
81 The *T. gondii* VAC also possesses transmembrane proteins, including an orthologue of the
82 *Plasmodium falciparum* chloroquine resistance transporter (PfCRT) (15). *Arabidopsis*
83 *thaliana* expresses a homologue of PfCRT as well, which is involved in export of
84 glutathione from plant chloroplasts (16). Similarly, PfCRT has been implicated in the
85 transport of amino acids and peptides out of the digestive vacuole, and is also important
86 for efflux of chloroquine from the malaria digestive vacuole to the parasite cytosol (17).
87 Recent work utilizing yeast demonstrated that *T. gondii* CRT (TgCRT) is also capable of
88 transporting chloroquine (18). Thus, similar to PfCRT, *T. gondii* CRT (TgCRT) might also
89 transport small amino acids and peptides out of the *T. gondii* VAC and into the parasite
90 cytosol. Two studies have revealed that *T. gondii* RH tachyzoites deficient in TgCRT,
91 either by inducible knockdown or complete genetic ablation, exhibit an enlarged VAC (15,
92 18). In addition, expansion of the VAC in TgCRT deficient tachyzoites is diminished when
93 parasite digestion is impaired by genetic ablation of cathepsin protease B (TgCPB) or
94 chemical inhibition of TgCPL with LHVS (18). Thus, the distended VAC in TgCRT deficient
95 tachyzoites was postulated to be due to increased osmotic pressure from a buildup of
96 digestion products that could not be transported out of the VAC (15, 18). TgCRT deficient

tachyzoites also grow more slowly *in vitro* and are compromised in their ability to cause mortality in mice during acute infection, suggesting an inability to transport digested material out of the VAC and into the parasite cytosol has a moderate effect on *T. gondii* tachyzoites (15, 18)

However, the extent to which TgCRT functions as a transporter of digestion products in bradyzoite cysts and thereby contributes to VAC morphology or function, or whether it is necessary for parasite viability during the chronic stage of infection, is unknown. We therefore sought to define the function of TgCRT in bradyzoites and its contribution to bradyzoite survival. To study this, we created a knockout of TgCRT in a cystogenic strain and assessed VAC morphology, *in vitro* and *in vivo* viability, and VAC digestion of host- or parasite-derived material in TgCRT deficient bradyzoites. We show that these bradyzoites exhibit a severely bloated VAC, that TgCRT appears to function downstream of protein digestion within the VAC, and that TgCRT deficiency results in loss of bradyzoite viability.

RESULTS

PΔ*crt* parasites exhibit a markedly distended VAC. To examine the role of TgCRT in bradyzoites, we knocked out TgCRT in the cystogenic type II Prugniaud strain (PΔ*crt*) and restored its expression via genetic complementation (PΔ*crt:CRT*) (Fig. S1 & S2). Consistent with TgCRT playing a role in VAC morphology, PΔ*crt* extracellular tachyzoites (Fig. 1A) and bradyzoites isolated from *in vitro* cysts (Fig. 1B) show a larger translucent vacuole associated with the VAC marker TgCPL than the parental and complement strains. The translucent vacuole was also observed within intact *in vitro* TgCRT deficient bradyzoite cysts, as seen by phase contrast (Fig. 1C) and electron microscopy (EM) (Fig.

1D), suggesting VAC enlargement in bradyzoites is not strictly a consequence of being in an extracellular environment. Quantification of EM images reveals a 5-fold enlargement of VAC area in PΔ*crt* bradyzoites as compared with the parental and complement strains (Fig. 1E). These results indicate that TgCRT deficiency in a cystogenic type II strain results in a pronounced enlargement of the VAC in both tachyzoites and bradyzoites.

TgCRT is required for *in vitro* bradyzoite viability and *in vivo* cyst burden. Previous work established that proteolytic digestion of material in the VAC is necessary for survival of *T. gondii* bradyzoites *in vitro* and *in vivo* (13). Because TgCRT is important for maintaining normal VAC morphology, we reasoned that TgCRT deficiency might compromise bradyzoite viability. We first wanted to address whether the lack of TgCRT affected the rate or efficiency of tachyzoite to bradyzoite conversion and bradyzoite replication. The parasite strains used express GFP under the early bradyzoite LDH2 promoter (19). To assess conversion, we measured the percentage of parasite-containing vacuoles that were greater than 50% positive for GFP or the more mature stage bradyzoite specific marker TgBAG1 over the first 4 days of conversion. For both early- and mature-bradyzoite stage markers analyzed, we found that all strains converted at a similar rate (Fig. S3). In addition, we measured the cyst size as an indicator of bradyzoite replication at 1 and 2 weeks post-conversion and found them to be comparable amongst all strains at both time points (Fig. S4). These findings suggest that TgCRT is not necessary for acute to chronic stage differentiation or replication of chronic stage parasites up to 2 weeks *in vitro*.

144 We then sought to assess the extent to which TgCRT deficiency affects bradyzoite viability
145 *in vitro*. First we measured the expression of GFP as a proxy of bradyzoite health. It was
146 previously shown that as bradyzoite viability decreases, there is a shift from cysts being
147 uniformly GFP positive to partially positive (mixture of GFP positive and GFP negative) to
148 fully GFP negative (13). Although we found that PΔ*crt* cysts were uniformly GFP positive
149 (Fig. 2A) the intensity of GFP was diminished at 2 weeks, but not 1 week, post-conversion
150 (Fig. 2B), suggesting a temporal decrease in gene expression. Next we more directly
151 evaluated bradyzoite viability using a qPCR/plaque assay (13), which measures the ability
152 of bradyzoites to initiate plaque formation relative to the inoculum (plaques/1000
153 genomes). We found that PΔ*crt* bradyzoite viability was decreased at 2 weeks, but not 1
154 week, post-conversion (Fig. 2C), mirroring the findings for GFP intensity. As a decrease in
155 plaques/genomes could be attributed to a deficiency in the ability of PΔ*crt* parasites to form
156 plaques, we conducted a tachyzoite plaque assay that revealed PΔ*crt* tachyzoites have no
157 deficit in the number of plaques formed (Fig. S5). Together these findings indicate a
158 progressive loss of PΔ*crt* bradyzoite viability *in vitro*.
159
160 To determine whether deletion of TgCRT affects the chronic infection *in vivo* we infected
161 C57BL/6 mice and enumerated brain cysts at 4 weeks post-infection. Mice inoculated with
162 PΔ*crt* tachyzoites showed a ~10-fold decrease in brain cyst burden compared with those
163 inoculated with the parental or complement strains (Fig. 3A). The reduction in cyst burden
164 was not due to a lack of infection since all mice were seropositive for *T. gondii* IgG,
165 including those in which no cysts were observed (Fig. 3B). However, it is possible that the
166 reduced number of PΔ*crt* brain cysts observed was due to fewer tachyzoites entering the
167 brain during acute infection. To examine this, we used qPCR to measure initial levels of

infection in the brain at days 7 and 10 post-infection. Compared to those infected with parental or complement strains, mice infected with PΔ*crt* parasites showed a 2-3 fold lower brain burden, suggesting that the decrease in cyst burden at 5 weeks post-infection is partly attributable to lower initial infection of the brain.

Because we found that *in vitro* TgCRT deficient bradyzoites are less viable, we wanted to examine whether residual *in vivo* PΔ*crt* cysts are infectious. To test this, we inoculated naïve mice with 5 or 30 cysts from the brains of mice chronically infected with Pru, PΔcrt, or PΔ*crt:CRT*. Once in the chronic phase, infection of naïve mice was monitored via serology and by determining whether parasites could be cultured from their brain homogenates. To serve as a negative control, 5 naïve mice were inoculated with brain homogenate from an uninfected mouse. All mice inoculated with PΔ*crt* brain cysts were seropositive, indicating that PΔ*crt* cysts contain infectious bradyzoites (Fig. 3D). However, only 50% of the seropositive mice were culture positive. In contrast, while not all mice inoculated with parental or complement brain cysts were seropositive, parasites were cultured from the brains of 100% of the seropositive mice. Taken together, our *in vitro* and *in vivo* data indicate that TgCRT deficient bradyzoites show a decrease, but not absolute loss, of viability.

Digestion in the VAC of TgCRT deficient tachyzoites and bradyzoites. We next wanted to interrogate whether the decreased viability in TgCRT deficient bradyzoites is possibly due to an impairment of proteolytic digestion in the VAC. Pru strain tachyzoites and bradyzoites deficient in the VAC protease TgCPL (PΔ*cpl*) have a deficit in digestion and reduced bradyzoite viability (13). It was recently suggested that RHΔ*crt* tachyzoites

192 have 25% less TgCPL, but the extent to which this affects VAC digestion was not
193 assessed (18). To probe whether TgCRT deficiency affects VAC digestion in tachyzoites,
194 we utilized a tachyzoite ingestion/digestion assay that permits the detection of ingested
195 and undigested host-derived mCherry within tachyzoites (12). We included PΔ*cpl* as a
196 reference control since these parasites accumulate host-derived mCherry due to a
197 deficiency in VAC proteolytic activity (11, 13, 14). We also created a PΔ*crt*Δ*cpl* double
198 knockout strain by ablating TgCRT in the PΔ*cpl* strain to determine whether a lack of
199 accumulated host-derived material in PΔ*crt* parasites is due to functional digestion or
200 problems in protein delivery to the VAC (Fig. S1). Western blotting confirmed that TgCPL
201 was expressed in all strains except for PΔ*cpl* and PΔ*crt*Δ*cpl* (Fig. 4A). Accumulation of
202 host-derived mCherry was observed in tachyzoites of all strains (Fig. 4B). However, we
203 found that whereas 33% of PΔ*cpl* and 38% PΔ*crt*Δ*cpl* tachyzoites accumulated host-
204 derived mCherry, PΔ*crt* showed only 3% mCherry positive tachyzoites, which is
205 comparable to the parental and complement lines (Fig. 4C). Accumulation of mCherry in
206 PΔ*crt*Δ*cpl* parasites was not significantly different than that of PΔ*cpl*. Taken together, these
207 findings suggest that TgCRT is not required for the delivery or digestion of host-derived
208 protein in the VAC of tachyzoites.
209
210 We next wanted to determine whether TgCRT deficiency affects VAC digestion in
211 bradyzoites. Since it has not yet been shown whether bradyzoites are capable of ingesting
212 host cytosolic material akin to tachyzoites, we instead employed a 'puncta' assay to initially
213 assess VAC digestion in bradyzoites. This assay is based on a previous report showing
214 that disruption of VAC proteolysis with the TgCPL inhibitor LHVS leads to the accumulation
215 of undigested material in the VAC, which is visible by phase contrast microscopy as dark

puncta (13). We found that PΔ*crt* cysts treated with LHVS developed dark puncta and that this corresponded with loss of the translucent VAC (Fig. 5A and B). As expected, there was an increase in dark puncta of parental and complement LHVS treated cysts as well. However, PΔ*crt* cysts contain larger dark puncta in both DMSO and LHVS treated samples than in the parental and complement cysts (Fig. 5B). Also, although PΔ*crt* bradyzoites did not show an increase in the total number of puncta (Fig. 5C), the percentage of total cyst area occupied by puncta was increased with LHVS treatment (Fig. 5D). Together these findings suggest that PΔ*crt* bradyzoites have larger puncta as an indicator of undigested material; however, whether this is a result of moderately impaired proteolytic digestion within the VAC or the intrinsically larger size of PΔ*crt* VAC is unclear.

The dark puncta observed within LHVS-treated bradyzoite cysts have been shown to co-localize with TgCPL and *T. gondii* autophagy-related protein 8 (TgAtg8), suggesting that some of the undigested material found within the bradyzoite VAC is derived from autophagy (13). To interrogate whether TgCRT deficiency affects the production or turnover of parasite autophagosomes, we created a PΔ*crt* strain that ectopically expresses tdTomato-TgAtg8 (Fig. S2), as done previously for Pru (13). Abundance of tdTomato-TgAtg8 in DMSO treated bradyzoites is a function of autophagosomal production and turnover. By contrast, tdTomato-TgAtg8 abundance in LHVS treated bradyzoites is a function of autophagosomal production exclusively since turnover is blocked. Pru- and PΔ*crt* tdTomato-TgAtg8 cysts treated with DMSO or LHVS for 1 or 3 days were assessed for tdTomato-TgAtg8 intensity both within cysts and in isolated bradyzoites. We also measured the total area of tdTomato-TgAtg8 puncta within cysts. For the DMSO control, no significant differences were seen between Pru and PΔ*crt* parasites for tdTomato-

TgAtg8 intensity in intact cysts (Fig. 6A & B) or isolated bradyzoites (Fig. 6C), suggesting no change in the balance of autophagosome production and turnover. DMSO treated PΔ*crt* bradyzoites showed a modest, but significant, increase in tdTomato-TgAtg8 puncta size (Fig. 6D), potentially due to tdTomato-TgAtg8 association with the enlarged VAC in such parasites. Upon inhibition of VAC proteolysis with LHVS, tdTomato-TgAtg8 intensity and size increased progressively for both Pru and PΔ*crt* bradyzoites. However, accumulation of tdTomato-TgAtg8 in PΔ*crt* bradyzoites was delayed and somewhat muted compared to Pru. Taken together, these data suggest that the balance of autophagosome production and turnover is unchanged in PΔ*crt*, but that TgCRT deficiency is associated an overall lower rate of autophagosome production.

TgCRT transport function is linked to VAC proteolysis. Malaria parasites bearing chloroquine resistance mutations in PfCRT display an enlarged digestive vacuole and they accumulate small peptides derived from hemoglobin (20, 21). This combined with other work showing that recombinant PfCRT transports amino acids, small peptides, and chloroquine (17) suggests that PfCRT functions to transport products of hemoglobin digestion out of the digestive vacuole. More recently, TgCRT was also shown to transport chloroquine upon heterologous expression in yeast (18). It is therefore plausible that TgCRT is also able to transport amino acids and small peptides out of the VAC. If TgCRT plays a similar role and the swelling of the VAC in *P*Δ*crt* parasites is due to a buildup of TgCRT substrates derived from protein digestion, then reducing the production of digestion products by inhibiting TgCPL should prevent or reverse VAC enlargement.

263 To test this, we differentiated PΔ*crt* bradyzoites 7 days before adding LHVS for another 2
264 days under differentiation conditions. This treatment window was chosen because our
265 earlier results showed that 3 days of LHVS treatment results in larger dark and Atg8
266 puncta areas (Fig. 5B & 6D), whereas a 1 day treatment appeared to have no notable
267 effect on Atg8 intensity (Fig. 5B & C). We reasoned that with 2 days of treatment, we
268 should begin seeing an effect of LHVS treatment on VAC size prior to excessive
269 accumulation of undigested protein. Although some enlarged VACs were apparent in
270 LHVS treated PΔ*crt* bradyzoites (Fig. 7A), quantification revealed a significant restoration
271 of VAC size upon LHVS treatment (Fig. 7B). Also, undigested material accumulated within
272 the VAC of PΔ*crt* bradyzoites treated with LHVS, suggesting that TgCPL is active in PΔ*crt*
273 bradyzoites.
274
275 To validate a link between TgCRT transport function and VAC proteolysis, we compared
276 the size and appearance of the VAC in PΔ*crt* bradyzoites with that of Pru or PΔ*crt*Δ*cpl*
277 parasites. We found that after 4 or 7 days of conversion to bradyzoite cysts, PΔ*crt*Δ*cpl*
278 bradyzoites have visually smaller VACs full of electron-dense, undigested material
279 compared to the markedly enlarged, more electron-lucent VACs of PΔ*crt* bradyzoites (Fig.
280 7C). Quantification revealed VAC size of PΔ*crt*Δ*cpl* strains to be significantly smaller than
281 PΔ*crt* VACs at both time points (Fig. 7D). These findings indicate that by genetically
282 limiting proteolysis in the VAC, the gross enlargement of the VAC observed in PΔ*crt*
283 bradyzoites is prevented. In addition, whereas approximately 20% PΔ*crt* cysts were dead
284 or dying at both 4 and 7 days post-conversion, 75% of PΔ*crt*Δ*cpl* cysts were degenerate at
285 4 days and 100% were degenerate at 7 days post-conversion. Thus, parasite lacking both
286 TgCRT and TgCPL appear to be more severely compromised than those lacking TgCRT

287 alone. Taken together, our findings suggest a link between TgCRT and protein digestion in
288 a manner that is consistent with TgCRT acting as an exporter of degradation products
289 generated by VAC proteases in bradyzoites.
290
291 **DISCUSSION**
292 Herein we show that TgCRT is necessary for maintaining the size of the VAC and the
293 viability of *T. gondii* bradyzoites, possibly by functioning as a transporter of digested
294 material from the VAC to the parasite cytosol. Together with other recent studies reporting
295 that VAC protein digestion is crucial for bradyzoite viability (13), our findings point toward
296 the VAC as an important organelle for *T. gondii* bradyzoite persistence and uncover
297 TgCRT as a potential target for chronic *T. gondii* infection.
298
299 Our finding that deletion of TgCRT in a type II strain (PΔ*crt*) resulted in enlargement of the
300 VAC is in line with previous studies that have knocked down (15) or knocked out (18)
301 TgCRT in a type I strain (RH). We also show that this enlarged VAC phenotype is
302 consistent across life stages and that it appears to be especially prominent in bradyzoites.
303 Our EM measurements suggest that the VAC occupies one third of the cytoplasm of PΔ*crt*
304 bradyzoites, thus becoming easily visible by phase contract microscopy in many parasites.
305 VAC enlargement was fully reversed upon re-expression of TgCRT, firmly establishing that
306 TgCRT expression is necessary to maintain normal VAC morphology.
307
308 The underlying basis for enlargement of the VAC in TgCRT deficient parasites is unknown,
309 but may be linked to endolysosomal system dynamics and the transporter function of
310 TgCRT. The VAC is a dynamic organelle that undergoes rounds of fission to form smaller

311 structures late in the cell cycle before fusing to form typically a single compartment in G1
312 phase (10, 22). The VAC probably also communicates via fusion and fission with the
313 parasite endosome-like compartments (ELCs), based on partial colocalization of VAC and
314 ELC markers in intracellular parasites (10, 18, 22). Interestingly, it was recently reported
315 that replicating PΔ*crt* parasites maintain a single VAC that overlaps substantially with ELC
316 markers (18). These findings imply that defects in VAC fragmentation and fission of the
317 VAC from the ELCs result in sustaining a hybrid VAC/ELC compartment in parasites
318 lacking TgCRT. Thus, contributions of membrane from both the VAC and ELCs could
319 account for enlargement of the VAC in PΔ*crt* parasites. Although it is possible that TgCRT
320 directly participates in vesicular fission, no evidence of this currently exists. On the other
321 hand, it appears more likely that swelling of the VAC in TgCRT deficient parasites is
322 related to TgCRT transport function. If, akin to PfCRT, TgCRT exports proteolytic digestion
323 products from the VAC, accumulation of such products in the VAC of PΔ*crt* parasites could
324 increase osmotic pressure within the organelle due to the influx of water through a VAC-
325 localized aquaporin (22). Whether a build-up of osmotic pressure is a driver of VAC size in
326 TgCRT deficient parasites and is thereby responsible for defective VAC fragmentation and
327 VAC/ELC resolution awaits further study.
328
329 A knockout of *Plasmodium* CRT has not been reported, presumably because of it having
330 an essential function. Nevertheless, chloroquine resistant strains bearing mutations in
331 PfCRT also exhibit an enlarged digestive vacuole. Studies with recombinant PfCRT
332 suggested that chloroquine resistant alleles tend to have lower transport activity for a
333 model substrate (tetraethyl ammonium), but higher transport activity for chloroquine (17).
334 Chloroquine resistant strains also accumulate small peptides derived from digestion of

335 hemoglobin (20, 21). Thus, the enlarged digestive vacuole of chloroquine resistant strains
336 is potentially due to a partial loss of PfCRT native transport function. That PfCRT is
337 essential whereas TgCRT is dispensable likely reflects the crucial role of the malaria
338 digestive vacuole in detoxification of heme liberated from hemoglobin digestion during
339 replication within erythrocytes.
340
341 Consistent with an important role for TgCRT in chronic infection, we observed a ~5-fold
342 loss of viability for PΔ*crt* bradyzoites *in vitro*. Loss of viability appears to increase with time
343 of differentiation, suggesting a progressively important role for TgCRT in chronic infection.
344 We also noted a 10-fold decrease in PΔ*crt* brain cysts in mice. This decrease is likely a
345 composite of effects occurring during the acute stage and the chronic stage. The trend
346 toward lower initial infection of the brain observed for PΔ*crt* parasites is in agreement with
347 the decreased virulence reported during acute infection of RHΔ*crt* parasites (18). However,
348 the lower initial infection of the brain does not appear to fully account for the striking
349 decrease in PΔ*crt* brain cysts. Additional loss of PΔ*crt* cysts during the chronic infection of
350 mice is consistent with our *in vitro* viability findings. Nevertheless, we found that cysts
351 recovered from the brains of PΔ*crt* infected mice contained infectious bradyzoites capable
352 of establishing infection of naïve mice. Our observation of lower PΔ*crt* cultivation efficiency
353 from the brains of infected naïve mice is further evidence of a decreased brain burden
354 and/or viability. Thus, whereas TgCRT is not absolutely required for *T. gondii* persistence,
355 it nonetheless strongly influences the course and burden of chronic infection.
356
357 Proteolysis within the VAC is necessary for sustaining bradyzoite viability *in vitro* and *in*
358 *vivo* (13). Genetically or chemically disrupting TgCPL activity results in a loss of bradyzoite

359 viability that is associated with accumulation of undigested material co-localizing with Atg8,
360 a marker of autophagosomes. *P. falciparum* parasites administered protease inhibitors that
361 target digestive vacuole proteinases also accumulate undigested material, in this case
362 hemoglobin derived from the infected erythrocyte (20). However, the electron-lucent VACs
363 observed in PΔ*crt* parasites, along with the tachyzoite ingestion assay, dark puncta
364 measurements, and Atg8 accumulation data suggests that digestion in PΔ*crt* tachyzoites
365 and bradyzoites is largely normal despite the striking morphological changes to the
366 organelle. It was suggested that RHΔ*crt* tachyzoites reduce the expression of several VAC
367 proteases to decrease production of TgCRT substrates generated by VAC proteolysis,
368 thereby easing osmotic pressure (18). If VAC proteolysis is similarly reduced in PΔ*crt*
369 parasites, this does not appear to affect the digestion of host-derived protein in tachyzoites
370 via the ingestion pathway or parasite-derived material delivered through autophagy.
371
372 Consistent with TgCRT functioning as a transporter downstream of VAC proteolysis, we
373 found that treating PΔ*crt* bradyzoites with LHVS restored VAC size prior to subsequent
374 accumulation of undigested material. This was observed in the EM images with 2 days of
375 LHVS treatment, where VACs are smaller and a buildup of undigested material is
376 beginning to show. We also found that PΔ*crt*Δ*cpl* double knockout bradyzoites have a
377 normal sized VAC, confirming that protein digestion in the VAC is required for expansion of
378 the VAC in TgCRT deficient parasites. The accumulation of undigested material in LHVS
379 treated PΔ*crt* and PΔ*crt*Δ*cpl* is consistent with delivery of proteolytic substrates to the VAC
380 TgCRT deficient bradyzoites. Nevertheless, we noted a delay in the accumulation of the
381 autophagic marker TgAtg8 in PΔ*crt* bradyzoites after blocking TgCPL activity with LHVS,
382 suggesting a decrease in the production of autophagosomes. Whether this is a result of a

feedback loop to reduce delivery of substrates to the VAC akin to the down-regulation of proteases in TgCRT deficient tachyzoites (18) or a due to a general decline in the health of PΔ*crt* bradyzoites remains unclear. It should also be noted that although we were unable to introduce tdTomato-TgAtg8 into PΔ*crt:CRT* parasites due to a lack of available selectable markers, all of the other phenotypes measured in PΔ*crt* parasites were restored upon genetic complementation.

Previous work in TgCPL together with the current findings for TgCRT is consistent with a central role for the VAC in *T. gondii* persistence. Parasites deficient in TgCPL and TgCRT appear to be especially compromised, which is consistent with a functional link between these VAC components. Additional studies aimed at targeting these proteins and identifying new components of the VAC are needed to realize the potential of compromising this organelle for therapeutic gain.

MATERIALS AND METHODS

Host cell and parasite cultures. Human foreskin fibroblasts (HFFs) were grown in Dulbecco's Modified Eagle Medium (DMEM, Gibco) containing 10% cosmic calf (Gibco), 50 µg/ml penicillin-streptomycin, 2 mM L-glutamine, and 10 mM HEPES. *T. gondii* strains used in this study were derived from PruS/Luc strain (13) maintained *in vitro* by serial passage on human foreskin fibroblast (HFF) monolayers as previously described (23).

VAC staining. Egressed tachyzoites from HFFs were filter-purified and pelleted at 1500x*g* for 10 min. Parasites were settled on Cell-Tak™ (Fisher Scientific) coated slides for 30

min, fixed in 4% formaldehyde, and stained for with RbαTgCPL (1:500) and GtαRb 594 secondary (1:1000).

***In vitro* conversion**. Tachyzoites were converted to bradyzoite cysts *in vitro* using previously published methods (24). In brief, tachyzoites were allowed to invade HFFs overnight under standard growing conditions. Infected cells were then grown in alkaline media (RPMI 1540 w/o $NaHCO_3$, 50 mM HEPES, 3% FBS, Pen/Strep, pH 8.2) in an incubator without CO_2, with media changed every day until samples were processed.

Transmission electron microscopy. For ultrastructural observations of infected cells by thin-section, samples were fixed in 2.5% glutaraldehyde in 0.1 mM sodium cacodylate and processed as described (25). Ultra-thin sections of infected cells were stained with osmium tetraoxide before examination with Philips CM120 EM (Eindhoven, Netherlands) under 80 kV.

qPCR/plaque assay for bradyzoite viability. *In vitro* bradyzoite viability was assessed by plaque assays normalized to qPCR as previously described (13). Briefly, tachyzoites were converted to bradyzoite cysts for 7 and 14 days as described above. At these time points bradyzoites were harvested using pepsin treatment and added to HFF monolayers for 10 days, after which time plaques were counted. Genomic DNA was extracted from an aliquot of samples using the Qiagen Blood and Tissue Kit and SYBR Green qPCR performed using the primer pairs listed in Table S1 and the following reaction conditions: 98°C, 2’ [98°C, 5”; 68°C, 30”, 72°C, 45”] x 45 cycles.

GFP intensity . After 1 and 2 weeks of tachyzoite conversion, as described above, *in vitro* cysts were fixed and stained with biotinylated dolichos (primary; 1:400; Vector Laboratories) and Streptavidin Alexa350 (secondary; 1:1000; Life Technologies). Image J was used to select dolichos stained cysts and quantify the amount of GFP coverage and intensity within the cyst. The dolichos signal was used to create a mask for further analysis by auto thresholding with the Li method (26). Analysis under these masks was redirected to the GFP channel, where particles between 130 – 2300 μm^2 and 0.30-1.00 circularity were analyzed.

tdTomato-Atg8 intensity and size. After 1 week of tachyzoite conversion as described above, *in vitro* cysts were fixed and stained with biotinylated dolichos (primary; 1:400; Vector Laboratories) and Streptavidin Alexa350 (secondary; 1:1000; Life Technologies). ImageJ was used to select dolichos stained cysts and quantify the total intensity of tdTomato-Atg8 and the tdTomato-Atg8 puncta size within each cyst. Dolichos positive structures between 200-2000 μM^2 with a circularity of 0.40-1.00 were identified using the Minimum method of auto-thresholding. The resulting binary images were used to create masks under which Atg8 puncta were further analyzed. Td-Tomato Atg8 puncta were analyzed as being between 0.2-1.50 μM^2 with a circularity of 0.40-1.00 and were identified with the Phansalkar method of auto local thresholding with a radius of 15.

Tachyzoite plaque assay. Intracellular tachyzoites were harvested following standard procedures, counted, and added to HFF monolayers in triplicate to quadruplicate wells. Parasites were left undisturbed for 10 days, after which time plaques were counted.

455 **Mouse seropositivity.** *Toxoplasma* IgG was measured using enzyme linked
456 immunosorbent assay (ELISA) to determine infectivity. In brief, *Toxoplasma* lysate was
457 made from freshly lysed Pru tachyzoites that was sonicated in 1 ug/mL Leupeptin, 1 ug/mL
458 E64, TPCK, and 10 ug/mL A-PMSF. Plates were coated with 10 ng of antigen in coating
459 buffer (Na_2CO_3, $NaHCO_3$, pH 9.6) overnight, blocked in 3% gelatin/PBS-T, serum was
460 added in a 1:25 dilution in 1% gelatin/PBS-T and incubated for 1 hr at RT. Secondary
461 HRP-conjugated GtαMs (1:1000) was added for 1 hr. Substrate was added for color
462 development, which was stopped with H_2SO_4. Absorbance was read at 400 nm.
463
464 **Tachyzoite ingestion assay.** Tachyzoite digestion was determined using the ingestion
465 assay as previously described (12). In brief, inducible mCherry Chinese hamster ovary
466 (CHO) cells were plated and induced with 2 µg/mL of doxycycline for 5 days. Tachyzoites
467 were harvested from HFF cells and allowed to invade induced-CHO cells for 4 hrs.
468 Tachyzoites were then mechanically lysed out of host cells, purified, treated with pronase
469 and saponin, and imaged on Cell-Tak^{TM} (Fisher Scientific) coated slides. Samples were
470 coded at the time of initial harvesting. For each biological replicate, more than 200
471 tachyzoites of each genotype were analyzed for host-derived mCherry accumulation within
472 parasites.
473
474 **Western blotting.** Tachyzoite lysates were prepared from purified parasites with the
475 addition of boiled 1x sample buffer, and lysate from $3x10^5$ tachyzoites/10 µL sample buffer
476 was loaded onto 10% SDS polyacrylamide gels. Blots were probed with antibody to TgCPL
477 (Rb; 1:300) (10) and α-tubulin (Ms; 1:1000; Developmental Studies Hybridoma Bank,
478 University of Iowa) for the loading control.

Puncta measurements in LHVS treated parasites. Tachyzoites were converted to bradyzoite cysts as described above. After 7 days of conversion, parasites were treated with 1 μM LHVS or DMSO (control) every day for 3 days. Cells were then fixed and stained with biotinylated dolichos lectin (primary; 1:400; Vector Laboratories) and Streptavidin Alexa350 (secondary; 1:1000; Life Technologies). Image J was used to select dolichos stained cysts and quantify the number and size of puncta within the cyst. Images were automatically thresholded using the MaxEntropy method to create a binary image (27). Noise was reduced by opening the image with 6 iterations of one pixel. Masks were created by using the Analyze Particle function, with objects between 130 – 1900 μm^2, and a circularity of 0.30-1.00 begin called a cyst. Under these masks, dark puncta were analyzed in the following way: phase images were Guassian blurred with a sigma of 2, and then auto-local thresholding was performed using the Phansalkar method (28) with a radius of 5 pixels. Objects with an area of 0.20 – 6.00 μm^2 and a circularity of 0.50 – 1.00 were analyzed as dark puncta.

***In vitro* differentiation kinetics.** Tachyzoites were converted to bradyzoite cysts as described above. Parasites were fixed at 1, 2, 3, and 4 days post-conversion and stained for BAG1 (RbαBAG1, 1:1000), a late marker for bradyzoites. These parasites express GFP under the LDH2 promoter, an early marker of bradyzoites. Image J was used to analyze the BAG1 and GFP coverage of each vacuole. Vacuoles were manually identified using phase images by drawing an ROI with the freehand tool. The ROIs were then applied to other channels for analysis as follows. The GFP and Texas Red channels were auto-thresholded using optimal thresholding methods for each day of conversion. The non-

503 thresholded and thresholded ROIs were measured for pixel intensity and used to
504 determine overall and percent intensity for GFP and Texas Red. Vacuoles with over 50%
505 coverage were designated as being cysts, and the total percentage of GFP and BAG1
506 positive cysts was calculated independently.
507
508 **In *vivo* cyst burden.** C57BL/6J female mice (7-8 wks old, Jackson Laboratories, Bar
509 Harbor, ME) were used in this study. Mice were injected intra-peritoneum (i.p.) with purified
510 10^5 tachyzoites of either PruS/Luc (Pru), PruΔ*crt* (PΔ*crt*), or PruΔ*crt:CRT* (PΔ*crt:CRT*) in
511 200 µL of 1x phosphate-buffered saline (PBS). At 4 weeks post-infection (wpi) mice were
512 sacrificed following university-approved protocols. Brains were harvested and
513 homogenized in 1 mL ice-cold PBS via syringing through a 20-gauge needle. Mice were
514 coded and cysts were enumerated in 90 µL of brain homogenate (9% of the brain) and the
515 total brain cyst number calculated. Cyst burden data were pooled from 2 independent
516 experiments.
517
518 ***In vivo* parasite burden kinetics.** The same inoculation conditions as described for *in*
519 *vivo* cyst burden was used. At 7 and 10 days post-infection (dpi) mice were sacrificed and
520 brains harvested. Brains were homogenized in ice-cold PBS to have 50 ng homogenate/µL
521 PBS. gDNA was extracted from 50 µL of homogenate using the DNeasy Blood and Tissue
522 Kit (Qiagen). qPCR was performed in triplicate for each sample with the following cycling
523 conditions: 90°C, 2'; [98°C, 10"; 56°C, 20"; 72°C,20"]x45 using SSO Advanced SYBR
524 Green Supermix (BioRad), and 300 nM Tox9 and 11 primers listed in Table S1. *T. gondii*
525 standards of specified parasite numbers (1 – 10^5genomes/µL) were used to quantify
526 parasite brain burden.

***In vivo* cyst viability.** To determine the viability of *T. gondii* cysts procured from the *in vivo* cyst burden experiment, 5 and 30 brain cysts of Pru, P*Δcrt*, or P*Δcrt:CRT* were injected i.p. into C57BL/6J female mice (7-8 weeks old). Mice inoculated with an equivalent amount of uninfected mouse brain homogenate were used as a negative control for infection. At 3 wpi mice were coded and sacrificed. Serum and brain was collected as described above for the *in vivo* cyst burden. Half of each brain homogenate was added to confluent HFF cells and monitored for parasite growth for 4.5 weeks.

Flow cytometry. Parasites were fixed with 4% formaldehyde for 15 min at room temperature, washed one time with PBS and resuspended in PBS for analysis on a LSR Fortessa flow cytometer (BD Biosciences, San Jose, CA, USA) with BD FACSDiVa™ Software (BD Biosciences). Data were analyzed with FlowJo (BD Biosciences) using the following gating: FITC-positive parasites were characterized as bradyzoites; then, the amount of tdTomato-ATG8 in bradyzoites was determined by the 561 nm signal.

Statistics. Data was analyzed using GraphPad prism. For each data set, outliers were identified and removed using ROUT with Q=0.1%. Data was then tested for normality and equal variance. If passed, One-way ANOVA with Tukey's multiple comparisons was performed. If failed, Mann-Whitney U test or Kruskal-Wallis with Dunn's multiple comparison was performed.

ACKNOWLEDGEMENTS

This work was support by National Institutes of health grants R01AI060767 (to I.C.) and R01AI120627 (to V.B.C. and M.D.C.) and a grant from the Stanley Medical Research Institute (to V.B.C.).

We thank the excellent technical staff of the Electron Microscopy Core Facility at the Johns Hopkins University School of Medicine Microscopy Facility. We also thank Professor Carla Emiliani for helpful discussions and support. We appreciate the technical assistance of Drs. Abimbola Kolawole and Carmen Mirabelli with flow cytometry.

REFERENCES

1. Commodaro AG, Belfort RN, Rizzo LV, Muccioli C, Silveira C, Burnier MN, Jr., Belfort R, Jr. 2009. Ocular toxoplasmosis: an update and review of the literature. Mem Inst Oswaldo Cruz 104:345-50.
2. Khan K, Khan W. 2018. Congenital toxoplasmosis: An overview of the neurological and ocular manifestations. Parasitol Int 67:715-721.
3. Ozgonul C, Besirli CG. 2017. Recent Developments in the Diagnosis and Treatment of Ocular Toxoplasmosis. Ophthalmic Res 57:1-12.
4. Winstanley P. 1995. Drug treatment of toxoplasmic encephalitis in acquired immunodeficiency syndrome. Postgrad Med J 71:404-8.
5. Torrey EF, Bartko JJ, Lun ZR, Yolken RH. 2007. Antibodies to Toxoplasma gondii in patients with schizophrenia: a meta-analysis. Schizophr Bull 33:729-36.
6. Okusaga O, Langenberg P, Sleemi A, Vaswani D, Giegling I, Hartmann AM, Konte B, Friedl M, Groer MW, Yolken RH, Rujescu D, Postolache TT. 2011. Toxoplasma

gondii antibody titers and history of suicide attempts in patients with schizophrenia. Schizophr Res 133:150-5.

7. Xiao J, Prandovszky E, Kannan G, Pletnikov MV, Dickerson F, Severance EG, Yolken RH. 2018. Toxoplasma gondii: Biological Parameters of the Connection to Schizophrenia. Schizophr Bull 44:983-992.

8. Tyebji S, Seizova S, Hannan AJ, Tonkin CJ. 2018. Toxoplasmosis: A pathway to neuropsychiatric disorders. Neurosci Biobehav Rev 96:72-92.

9. Montoya JG, Liesenfeld O. 2004. Toxoplasmosis. Lancet 363:1965-76.

10. Parussini F, Coppens I, Shah PP, Diamond SL, Carruthers VB. 2010. Cathepsin L occupies a vacuolar compartment and is a protein maturase within the endo/exocytic system of Toxoplasma gondii. Mol Microbiol 76:1340-57.

11. Dou Z, McGovern OL, Di Cristina M, Carruthers VB. 2014. Toxoplasma gondii ingests and digests host cytosolic proteins. MBio 5:e01188-14.

12. McGovern OL, Rivera-Cuevas Y, Kannan G, Narwold AJ, Jr., Carruthers VB. 2018. Intersection of endocytic and exocytic systems in Toxoplasma gondii. Traffic 19:336-353.

13. Di Cristina M, Dou Z, Lunghi M, Kannan G, Huynh MH, McGovern OL, Schultz TL, Schultz AJ, Miller AJ, Hayes BM, van der Linden W, Emiliani C, Bogyo M, Besteiro S, Coppens I, Carruthers VB. 2017. Toxoplasma depends on lysosomal consumption of autophagosomes for persistent infection. Nat Microbiol 2:17096.

14. Larson ET, Parussini F, Huynh MH, Giebel JD, Kelley AM, Zhang L, Bogyo M, Merritt EA, Carruthers VB. 2009. Toxoplasma gondii cathepsin L is the primary target of the invasion-inhibitory compound morpholinurea-leucyl-homophenyl-vinyl sulfone phenyl. J Biol Chem 284:26839-50.

15. Warring SD, Dou Z, Carruthers VB, McFadden GI, van Dooren GG. 2014. Characterization of the chloroquine resistance transporter homologue in Toxoplasma gondii. Eukaryot Cell 13:1360-70.

16. Maughan SC, Pasternak M, Cairns N, Kiddle G, Brach T, Jarvis R, Haas F, Nieuwland J, Lim B, Muller C, Salcedo-Sora E, Kruse C, Orsel M, Hell R, Miller AJ, Bray P, Foyer CH, Murray JA, Meyer AJ, Cobbett CS. 2010. Plant homologs of the Plasmodium falciparum chloroquine-resistance transporter, PfCRT, are required for glutathione homeostasis and stress responses. Proc Natl Acad Sci U S A 107:2331-6.

17. Juge N, Moriyama S, Miyaji T, Kawakami M, Iwai H, Fukui T, Nelson N, Omote H, Moriyama Y. 2015. Plasmodium falciparum chloroquine resistance transporter is a H+-coupled polyspecific nutrient and drug exporter. Proc Natl Acad Sci U S A 112:3356-61.

18. Thornton LB, Teehan P, Floyd K, Cochrane C, Bergmann A, Dou Z. 2018. The ortholog of chloroquine resistance transporter (TgCRT) plays a key role in maintaining the integrity of the endolysosomal system in Toxoplasma gondii to facilitate host invasion. bioRxiv doi:10.1101/409904:409904.

19. Fox BA, Falla A, Rommereim LM, Tomita T, Gigley JP, Mercier C, Cesbron-Delauw MF, Weiss LM, Bzik DJ. 2011. Type II Toxoplasma gondii KU80 knockout strains enable functional analysis of genes required for cyst development and latent infection. Eukaryot Cell 10:1193-206.

20. Rosenthal PJ, McKerrow JH, Aikawa M, Nagasawa H, Leech JH. 1988. A malarial cysteine proteinase is necessary for hemoglobin degradation by Plasmodium falciparum. J Clin Invest 82:1560-6.

21. Pulcini S, Staines HM, Lee AH, Shafik SH, Bouyer G, Moore CM, Daley DA, Hoke MJ, Altenhofen LM, Painter HJ, Mu J, Ferguson DJ, Llinas M, Martin RE, Fidock DA, Cooper RA, Krishna S. 2015. Mutations in the Plasmodium falciparum chloroquine resistance transporter, PfCRT, enlarge the parasite's food vacuole and alter drug sensitivities. Sci Rep 5:14552.

22. Miranda K, Pace DA, Cintron R, Rodrigues JC, Fang J, Smith A, Rohloff P, Coelho E, de Haas F, de Souza W, Coppens I, Sibley LD, Moreno SN. 2010. Characterization of a novel organelle in Toxoplasma gondii with similar composition and function to the plant vacuole. Mol Microbiol 76:1358-75.

23. Di Cristina M, Ghouze F, Kocken CH, Naitza S, Cellini P, Soldati D, Thomas AW, Crisanti A. 1999. Transformed Toxoplasma gondii tachyzoites expressing the circumsporozoite protein of Plasmodium knowlesi elicit a specific immune response in rhesus monkeys. Infect Immun 67:1677-82.

24. Lunghi M, Galizi R, Magini A, Carruthers VB, Di Cristina M. 2015. Expression of the glycolytic enzymes enolase and lactate dehydrogenase during the early phase of Toxoplasma differentiation is regulated by an intron retention mechanism. Mol Microbiol 96:1159-75.

25. Coppens I, Joiner KA. 2003. Host but not parasite cholesterol controls Toxoplasma cell entry by modulating organelle discharge. Mol Biol Cell 14:3804-20.

26. Li CH, Tam PKS. 1998. An interative algorithm for minimum cross entropy thresholding. Pattern Recognition Letters 19:771-776.

27. Kapur JN, Sahoo PK, Wong AKC. 1985. A new method for gray-level picture thresholding using the entropy of the histogram. Computer Vision, Graphics, and Image Processing 29:273-285.

28. Phansalkar N, More S, Sabale A, Joshi MS. 2011. Adaptive local thresholding for detection of nuclei in diversity stained cytology images. International Conference on Communications and Signal Processing doi:10.1109/ICCSP.2011.5739305:218-220.

FIGURE LEGENDS

Figure 1. PΔ*crt* tachyzoites and bradyzoites exhibit a distended VAC.

A. Extracellular tachyzoites stained for the VAC protease TgCPL (red). Scale bar denotes 1 μM. Arrow denotes distended VAC.

B. Extracellular bradyzoites purified from *in vitro* cysts differentiated for 1 week and stained for TgCPL (red). Scale bar denotes 1 μM. Arrow denotes distended VAC.

C. Intracellular bradyzoite cysts differentiated *in vitro* for 1 week. Scale bar denotes 10 μM. Arrow denotes distended VAC.

D. Electron micrographs of intracellular bradyzoite cysts cultured *in vitro* for 1 week. Images within white boxes were expanded for the insets shown in the second row. Scale bars represent 500 nm for low magnification images and 200 nm for insets. P denotes the parasite.

E. Quantification of VAC size from electron micrographs. The following number of VACs were measured for each strain: Pru (13), PΔ*crt* (25), PΔ*crt:CRT* (15). Volume fraction corresponds to the area of the VAC/area of the parasite x 100. Bar is mean +/- SD. One-way ANOVA with Tukey's multiple comparisons was performed. **** denotes $p<0.0001$.

Figure 2. Deletion of CRT affects *in vitro* bradyzoite viability.

669 A. Fluorescent images of bradyzoite cysts expressing GFP under the early bradyzoite
670 LDH2 promoter after 1 and 2 weeks of *in vitro* differentiation. Scale bars denote 10
671 µM.
672 B. GFP intensity after 1 and 2 weeks of *in vitro* differentiation. Line represents mean
673 +/- S.D. of bradyzoite cysts in 3 independent experiments. The following number of
674 cysts were analyzed for each experiment for week 1: Pru (77, 54, 142), PΔ*crt* (54,
675 91, 148), PΔ*crt:CRT* (96, 92, 88) and for week 2: Pru (106, 124, 102), PΔ*crt* (56,
676 131, 94), PΔ*crt:CRT* (89, 107, 102). Kruskal Wallis with Dunn's multiple
677 comparisons was performed. **** denotes $p<0.0001$.
678 C. Viability of bradyzoites after 1 and 2 weeks of *in vitro* differentiation based on
679 plaque numbers normalized to qPCR quantification. Line represents mean +/- S.D.
680 of 3-4 technical replicates in 4-5 independent experiments. The following number of
681 technical replicates were analyzed for each experiment for week 1: Pru (3, 3, 3, 4,
682 4), PΔ*crt* (3, 3, 3, 4, 4), PΔ*crt:CRT* (3, 3, 3, 4) and for week 2: Pru (3, 3, 3, 4, 4),
683 PΔ*crt* (3, 3, 3, 4, 4), PΔ*crt:CRT* (3, 3, 3, 4, 4). Kruskal Wallis with Dunn's multiple
684 comparisons was performed. **** denotes $p<0.0001$ and * denotes $p<0.05$.
685
686 **Figure 3. Deletion of TgCRT affects *in vivo* bradyzoite burden.**
687 A. Brain cyst burden in mice at 4 weeks post-infection with *T. gondii*. Line represents
688 mean +/- S.D. of mice from 2 independent experiments. The total number of mice
689 analyzed were: Pru (12), PΔ*crt* (10), PΔ*crt:CRT* (15). Kruskal-Wallis with Dunn's
690 multiple comparisons was performed. *** denotes $p=0.0002$ and ** denotes $p=$
691 0.0098.

B. *T. gondii* IgG of mice infected in panel A. Age and sex-matched uninfected mice used as IgG negative control. One-way ANOVA with Holm-Sidak's multiple comparisons was performed. **** denotes $p<0.0001$, *** denotes $p=0.0002$, ** denotes $p=0.002$.

C. Brain parasite burden at 7 and 10 dpi. Line is mean +/- S.D. of mice from 2 independent experiments. Kruskal-Wallis with Dunn's multiple comparisons was performed. The following is the number of mice analyzed for 7 and 10 dpi respectively: Pru (10,11), PΔ*crt* (10,10), PΔ*crt:CRT* (9,10). ** denotes $p=0.005$, * denotes $p=0.017$.

D. *T. gondii* IgG levels in mice administered residual brain cysts (5 or 30 cysts). Data is from 1 experiment. Line is mean and dotted line is 2 SD above the mean of mice given uninfected brain homogenate. Open symbols denote mice administered 5 parasite cysts and closed symbols denote mice administered 30 parasite cysts. Red symbols denote no parasite growth from brain homogenate. The following is the total number of mice analyzed: Uninfected mice (4), Pru (6), PΔ*crt* (6), PΔ*crt:CRT* (6).

Figure 4. VAC digestive function is not altered in PΔ*crt* tachyzoites.

A. Western blot of tachyzoite lysates probed for TgCPL (~30 kDa) and α-Tubulin (~55 kDa) as loading control.

B. Representative images of tachyzoites with ingested host-derived mCherry in red. Scale bar denotes 1 μM.

C. Tachyzoite ingestion/digestion assay quantification from panel B. Lines represent the mean +/- SD of 3-4 experiments. The following numbers of tachyzoites were

716 enumerated for each experiment: Pru (234, 370, 280), PΔ*crt* (297, 258, 290, 241),
717 PΔ*crt:CRT* (235, 282, 239, 466), PΔ*crt*Δ*cpl* (268, 211, 270), PΔ*cpl* (426. 384, 275).
718 One-way ANOVA with Holm-Sidak's Multiple Comparisons was performed. ****
719 denotes $p<0.0001$.
720
721 **Figure 5. VAC digestive function is not altered in PΔ*crt* bradyzoites**
722 A. Representative images of bradyzoite cysts cultured *in vitro* for 7 days and then
723 treated with DMSO as a vehicle control or 1 μM LHVS for 3 days. Dark puncta are
724 clearly seen in LHVS treated cysts. Scale bar represents 5 μM and scale bar of
725 inset represents 1 μM.
726 B. Measurement of dark puncta area within cysts from 2-3 independent experiments.
727 Lines represent mean +/- S.D. The following number of cysts were analyzed from
728 each experiment: Pru DMSO (65, 68), Pru LHVS(66, 73), PΔ*crt* DMSO(72, 59, 69),
729 PΔ*crt* LHVS(109, 78, 70), PΔ*crt:CRT* DMSO(115, 60, 105), PΔ*crt:CRT* LHVS(77,
730 56, 94). Kruskal Wallis with Dunn's multiple comparisons was performed. ****
731 denotes $p<0.0001$, ** denotes $p<0.01$.
732 C. Total puncta number in cysts analyzed in B. Lines represent mean +/- S.D. The
733 following number of cysts were analyzed from each experiment: Pru DMSO (63,
734 64), Pru LHVS(63, 69), PΔ*crt* DMSO(70, 58, 66), PΔ*crt* LHVS(107, 74, 65),
735 PΔ*crt:CRT* DMSO(112, 58, 106), PΔ*crt:CRT* LHVS(73, 56, 87). Kruskal Wallis with
736 Dunn's multiple comparisons was performed.
737 D. Percent puncta coverage for each cyst analyzed in B. Lines represent mean +/-
738 S.D. Pru DMSO (65, 68), Pru LHVS(67, 73), PΔ*crt* DMSO(72, 59, 69), PΔ*crt*
739 LHVS(109, 78, 70), PΔ*crt:CRT* DMSO(113, 60, 106), PΔ*crt:CRT* LHVS(77, 56, 94).

740 Kruskal Wallis with Dunn's multiple comparisons was performed. **** denotes
741 $p<0.0001$.
742
743 **Figure 6. Autophagy in PΔ*crt* bradyzoites.**
744 A. Representative images of Pru and PΔ*crt* Atg8-tdTomato expressing strains after 7
745 days of conversion and treatment with DMSO or 1 μM LHVS for 1 or 3 days. Scale
746 bar represents 10 μM.
747 B. Total tdTomato-TgAtg8 intensity within parasite cysts converted and treated as in A.
748 Line represents mean +/- S.D. from 3-4 independent experiments. The following
749 number of cysts were analyzed in each experiment: Pru DMSO (46, 50, 26), Pru
750 LHVS 1 day (43, 47, 47, 16), Pru LHVS 3 day (45, 60, 31), PΔ*crt* DMSO (48, 54,
751 30), PΔ*crt* LHVS 1 day (37, 39, 58, 28), PΔ*crt* LHVS 3 day (59, 47, 16). Kruskal
752 Wallis with Dunn's multiple comparisons was performed. **** denotes $p<0.0001$, **
753 denotes $p<0.01$.
754 C. Atg8 intensity of bradyzoites analyzed by flow cytometry. Line represents mean +/-
755 S.D. from 3-4 independent experiments. The following number of bradyzoites that
756 were GFP and TdTomato positive were analyzed in each experiment: Pru DMSO
757 (1122, 5330, 1534), Pru LHVS 1 day (493, 3199, 613), Pru LHVS 3 day (1960,
758 5205, 2043), PΔ*crt* DMSO (620, 1115, 139), PΔ*crt* LHVS 1 day (623, 962, 230,
759 1355), PΔ*crt* LHVS 3 day (1802, 2641, 337). One-way ANOVA with Sidak's
760 multiple comparisons was performed. *** denotes $p<0.001$, ** denotes $p<0.01$, *
761 denotes $p<0.05$.
762 D. tdTomato-TgAtg8 puncta size was measured for every puncta in each cyst. Line
763 represents mean +/- S.D. from 3-4 independent experiments. The following number

of puncta were analyzed in each experiment: Pru DMSO (364, 290, 242), Pru LHVS 1 day (617, 301, 1826, 1147), Pru LHVS 3 day (722, 697, 1518, 36), PΔ*crt* DMSO (406, 427, 330), PΔ*crt* LHVS 1 day (277, 233, 484, 324), PΔ*crt* LHVS 3 day (692, 402, 633). Kruskal-Wallis with Dunn's multiple comparisons was performed. **** denotes $p<0.0001$.

Figure 7. VAC digestion disruption through CPL modulation affects PΔ*crt* bradyzoite VAC size and parasite health.

A. Electron microscopy of *in vitro* bradyzoite cysts converted for 7 days and then treated with DMSO and 1 μM LHVS for 2 days. Scale bars represent 500 nm.
B. Quantification of VACs in panel A. Bars represent mean +/- S.D. The following numbers of VACs were measured for each strain: Pru (18), PΔ*crt* DMSO (49), PΔ*crt* LHVS (13). One-way ANOVA with Tukey's multiple comparisons was performed. **** denotes $p<0.0001$, * denotes $p<0.05$.
C. Representative electron micrograph images of *in vitro* bradyzoite cysts converted for 4 day and 7 days. Scale bars represent 500 nm. P denotes parasite.
D. Quantification of VACs in panel C. Bars represent mean +/- S.D. The following number of VACs were measured for each strain: 4 day Pru (16), PΔ*crt* (17), PΔ*crt*Δ*cpl* (17). 7 day Pru (13), PΔ*crt* (25), PΔ*crt*Δ*cpl* (35). One-way ANOVA with Tukey's multiple comparisons was performed. **** denotes $p<0.0001$. 7 day Pru and PΔ*crt* data was also used in Figure 1.

SUPPLEMENTARY MATERIAL LEGENDS

Table S1. Primer sequences and PCR product sizes.

Figure S1. Targeted deletion of *CRT* in PRUΔku80 and PRUΔku80Δ*cpl*.

A. A vector carrying the BLE selection cassette flanked at both ends by 1500 bp of homologous regions upstream and downstream of the *CRT* gene was used to delete *CRT* by double cross-over homologous recombination.

B. Deletion of *CRT* was confirmed by PCR analyses using the primers indicated in each lane of the gel. Primer positions are shown in panel A. Primer sequences are provided in Table S1.

Figure S2: Genetic complementation of *CRT* and integration of dT-ATG8.

A. Complementation of *CRT* was accomplished by integrating a plasmid carrying the *CRT* cDNA cloned downstream of 1000 bp of *CRT* 5'UTR to drive transcription of these sequences. The plasmid was integrated upstream of the tubulin gene by introducing in the complement plasmid a 1425 bp fragment encompassing this locus and linearization using the *BclI* to induce single cross-over. The tdTomato-Tg Atg8 expression cassette was integrated in the tubulin locus of the Δ*crt* strain using the same strategy described for the *CRT* complementation strain.

B. Integration in the selected genome locus of the *CRT* complement or tdTomato-TgAtg8 plasmid was confirmed by PCR analysis. Primers used in these PCRs are indicated in panel A. Primer sequences are provided in Table S1.

Figure S3: *In vitro* differentiation kinetics.

Tachyzoite conversion into bradyzoite cysts was assessed over 4 days as determined by expression of GFP under the early bradyzoite promoter LDH2 or the

late bradyzoite marker BAG1 by IF staining. Bars are presented as mean +/- S.D. of 3 independent experiments. The following parasitophorous vacuoles (PVs) were assessed on days 1, 2, 3, 4, respectively. Experiment 1: Pru (88, 175, 187, 144), PΔ*crt* (113, 166, 186, 204), PΔ*crt:CRT* (87, 124, 189, 182). Experiment 2: Pru (73, 84, 200, 248), PΔ*crt* (88, 137, 205, 190), PΔ*crt:CRT* (59, 101, 109, 117). Experiment 3: Pru (64, 90, 69, 97), PΔ*crt* (80, 63, 135, 214), PΔ*crt:CRT* (65, 78, 96, 132). One-way ANOVA with Tukey's multiple comparisons was performed for comparing genotypes on each day.

Figure S4. CRT deficiency does not alter *in vitro* cyst size.

Cyst size after 1 and 2 weeks of *in vitro* differentiation. Line represents mean +/- S.D. of bradyzoite cysts in 3 independent experiments. The following number of cysts were analyzed for each experiment for week 1: Pru (78, 52, 142), PΔ*crt* (49, 90, 135), PΔ*crt:CRT* (89, 84, 87) and for week 2: Pru (111, 124, 102), PΔ*crt* (65, 131, 95), PΔ*crt:CRT* (90, 107, 102). Kruskal Wallis with Dunn's multiple comparisons was performed.

Figure 1

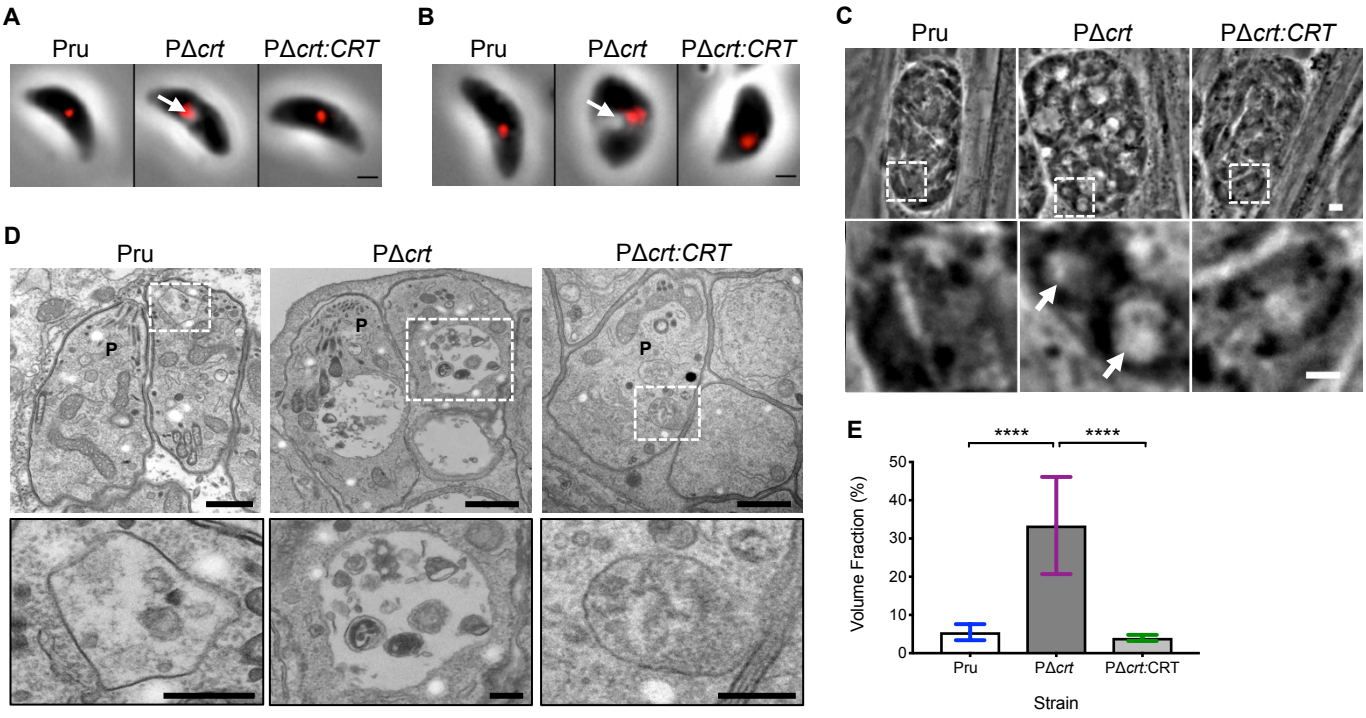
A
Pru
PΔcrt
PΔcrt:CRT
B
Pru
PΔcrt
PΔcrt:CRT
C
Pru
PΔcrt
PΔcrt:CRT
D
Pru
PΔcrt
PΔcrt:CRT
P
P
P
E
****
****
Volume Fraction (%)
50
40
30
20
10
0
Pru
PΔcrt
PΔcrt:CRT
Strain

Figure 2

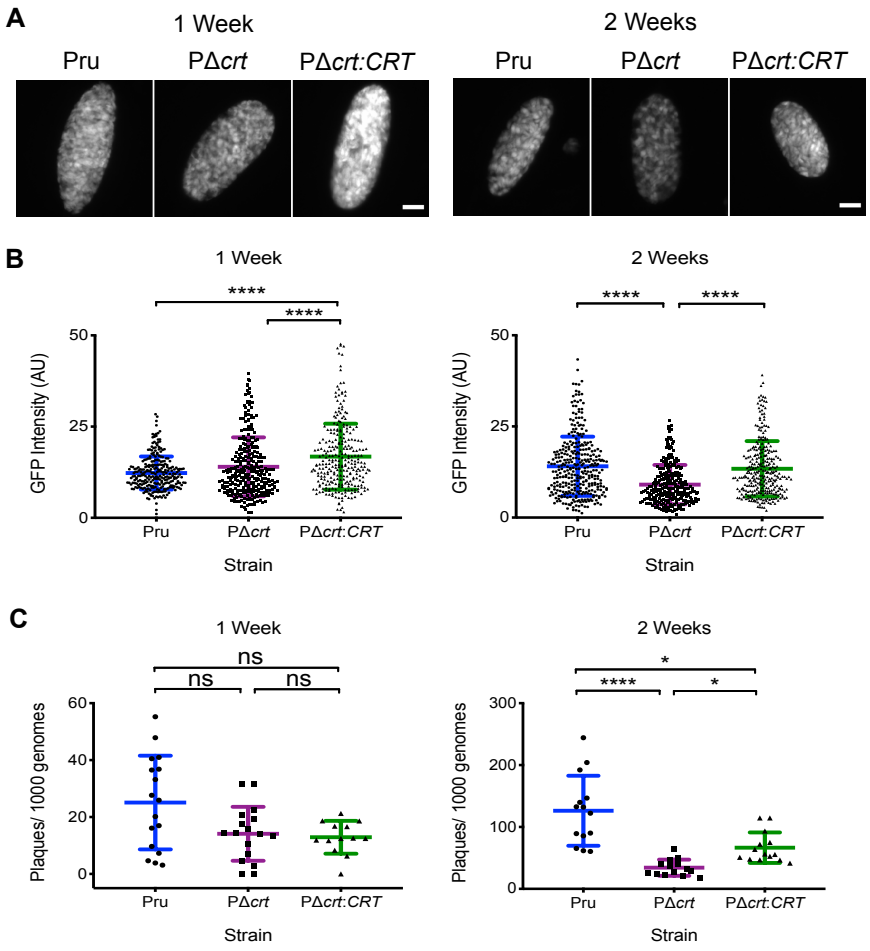
A
1 Week
2 Weeks
Pru
PΔcrt
PΔcrt:CRT
B
1 Week
2 Weeks
****
GFP Intensity (AU)
50
25
0
Pru
PΔcrt
PΔcrt:CRT
Strain
C
ns
*
Plaques/ 1000 genomes
60
40
20
300
200
100

Figure 3

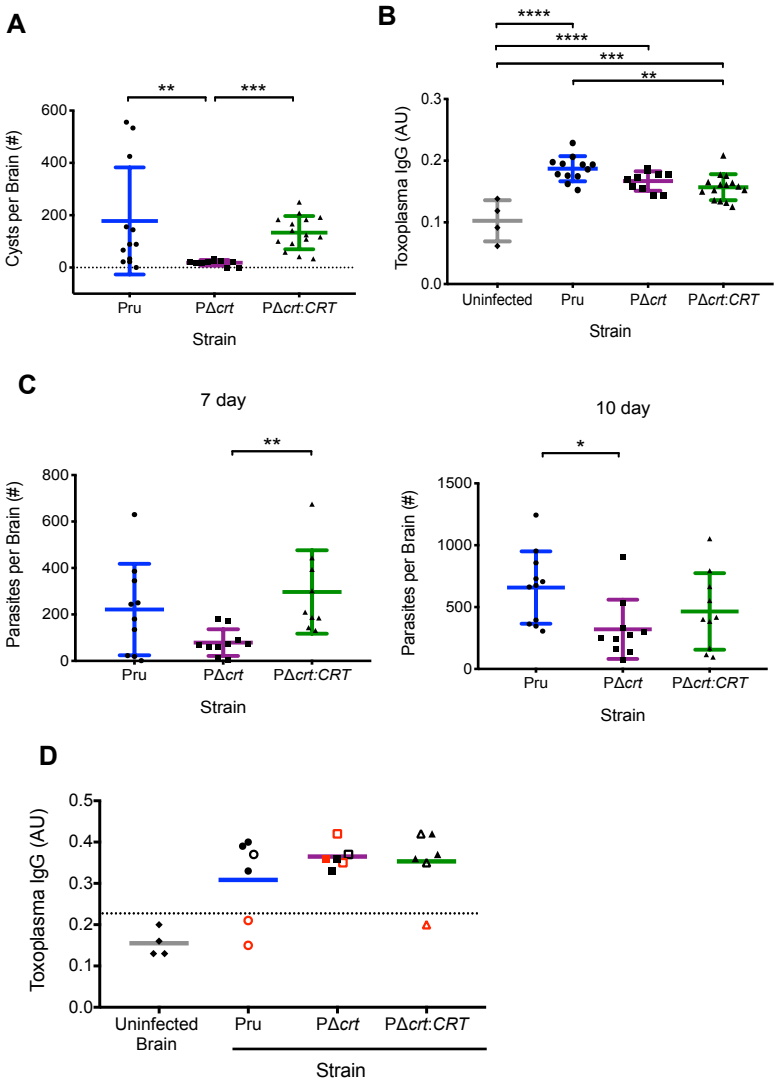
A
Cysts per Brain (#)
600
400
200
0
**
***
Pru
PΔcrt
PΔcrt:CRT
Strain
B
Toxoplasma IgG (AU)
0.3
0.2
0.1
0.0
****
****
***
**
Uninfected
Pru
PΔcrt
PΔcrt:CRT
Strain
C
7 day
Parasites per Brain (#)
800
600
400
200
0
**
Pru
PΔcrt
PΔcrt:CRT
Strain
10 day
Parasites per Brain (#)
1500
1000
500
0
*
Pru
PΔcrt
PΔcrt:CRT
Strain
D
Toxoplasma IgG (AU)
0.5
0.4
0.3
0.2
0.1
0.0
Uninfected Brain
Pru
PΔcrt
PΔcrt:CRT
Strain

Figure 4

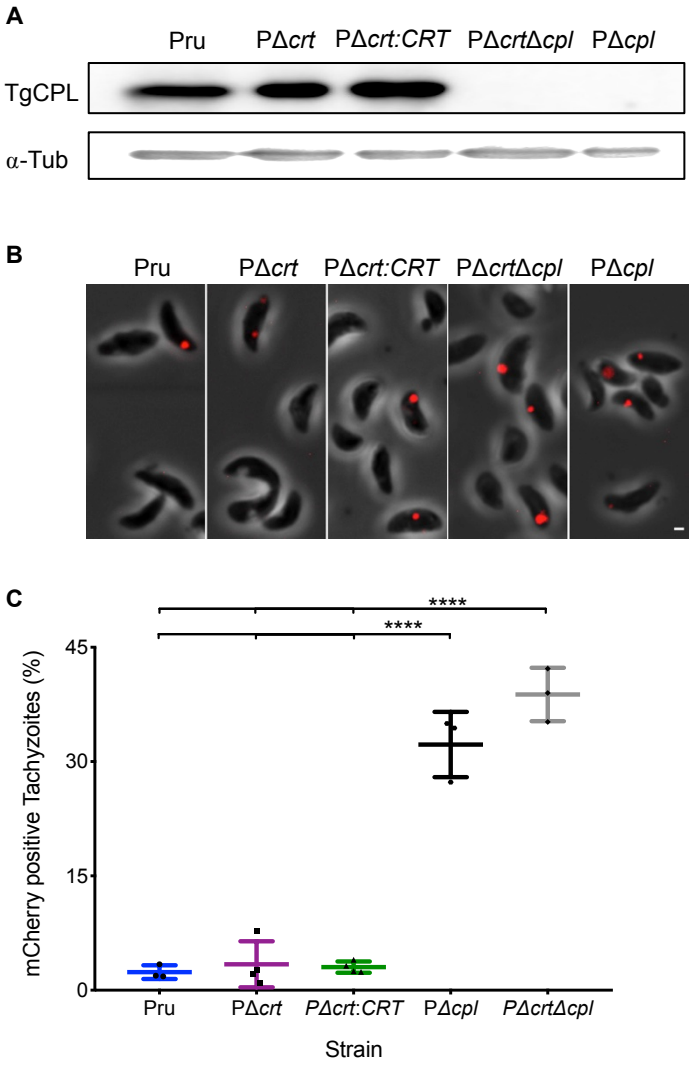
A
Pru
PΔcrt
PΔcrt:CRT
PΔcrtΔcpl
PΔcpl
TgCPL
α-Tub
B
Pru
PΔcrt
PΔcrt:CRT
PΔcrtΔcpl
PΔcpl
C
****
****
mCherry positive Tachyzoites (%)
45
30
15
0
Pru
PΔcrt
PΔcrt:CRT
PΔcpl
PΔcrtΔcpl
Strain

Figure 5

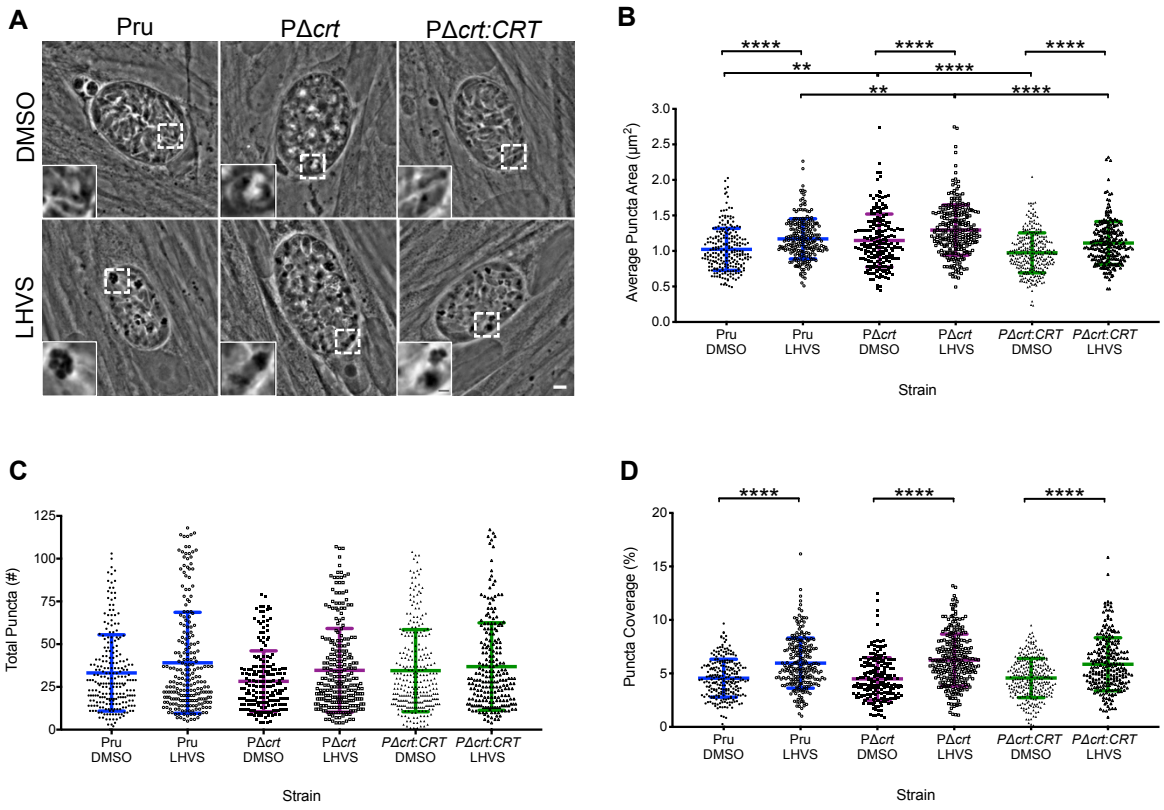
A
Pru
PΔcrt
PΔcrt:CRT
DMSO
LHVS
B
Average Puncta Area (μm²)
Pru DMSO
Pru LHVS
PΔcrt DMSO
PΔcrt LHVS
PΔcrt:CRT DMSO
PΔcrt:CRT LHVS
Strain
C
Total Puncta (#)
Strain
D
Puncta Coverage (%)
Strain

Figure 6

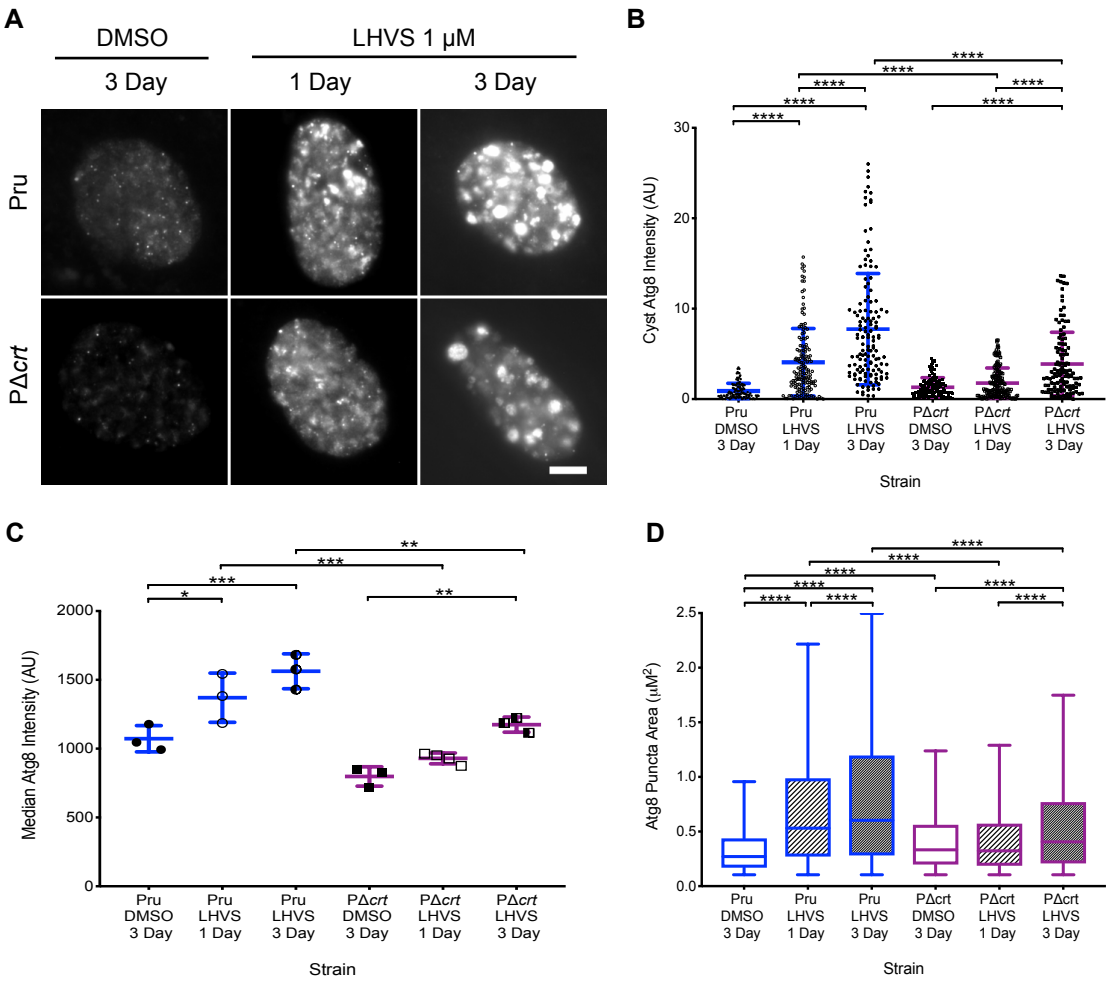
A
DMSO
LHVS 1 µM
3 Day
1 Day
3 Day
Pru
PΔcrt
B
Cyst Atg8 Intensity (AU)
Strain
Pru DMSO 3 Day
Pru LHVS 1 Day
Pru LHVS 3 Day
PΔcrt DMSO 3 Day
PΔcrt LHVS 1 Day
PΔcrt LHVS 3 Day
C
Median Atg8 Intensity (AU)
D
Atg8 Puncta Area (µM²)

Figure 7

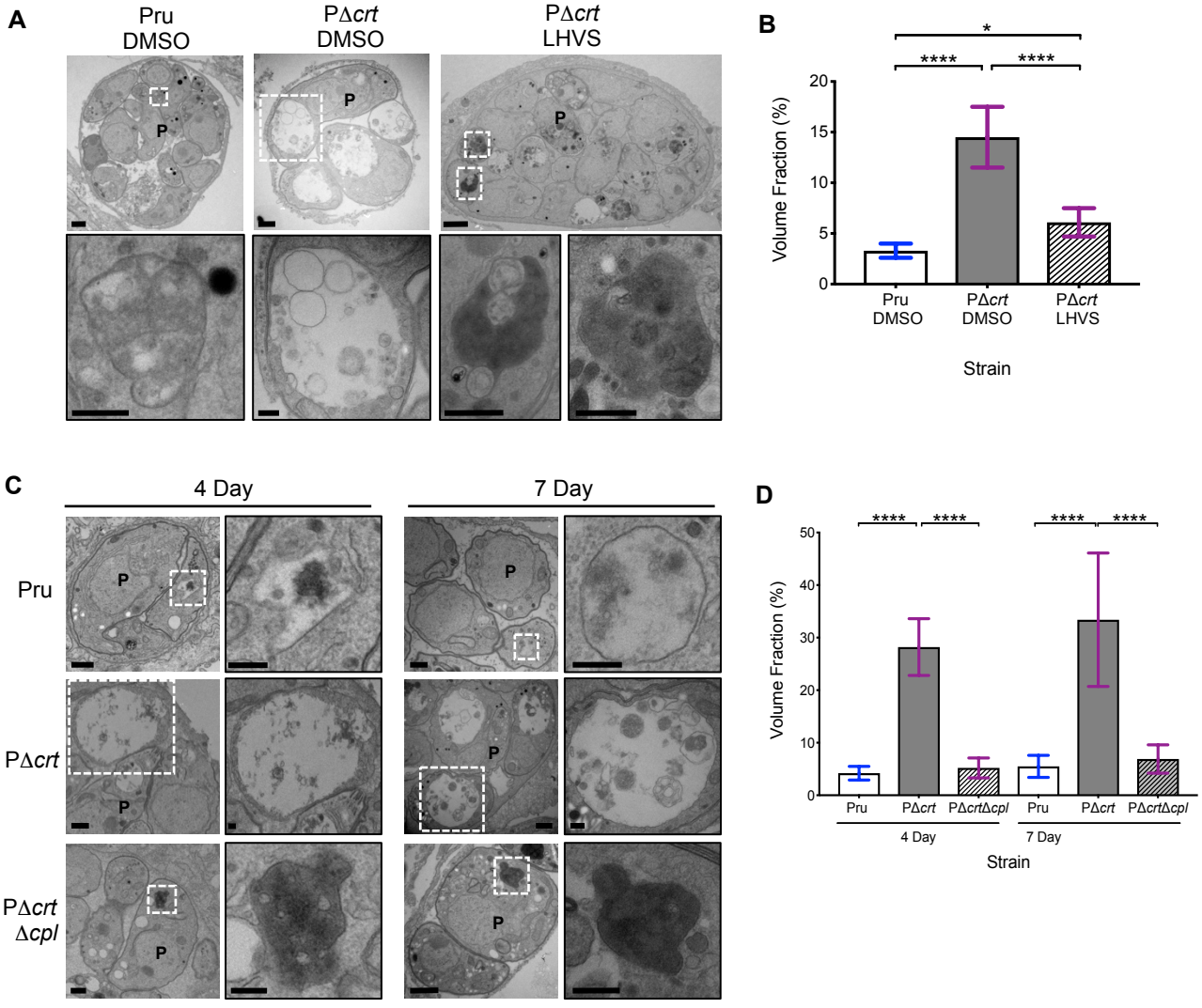
A
Pru DMSO
PΔcrt DMSO
PΔcrt LHVS
P
B
*
****
****
Volume Fraction (%)
20
15
10
5
0
Pru DMSO
PΔcrt DMSO
PΔcrt LHVS
Strain
C
4 Day
7 Day
Pru
PΔcrt
PΔcrt Δcpl
P
D
****
****
****
****
Volume Fraction (%)
50
40
30
20
10
0
Pru
PΔcrt
PΔcrtΔcpl
Pru
PΔcrt
PΔcrtΔcpl
4 Day
7 Day
Strain

Table S1

Primer Name	Forward Primer (5'- 3')	Reverse Primer (5'-3')	Product Size (bp)
Deletion of CRT (Fig. S1)			
5' ARM of CRT; upstream of BLE with *Xho*I/ *Hind*III sites	CCCCCTCGAGGTGCACCGTTTGACACATCTG ATTGTG	TTCGAAGCTTGTCGCGCTAGCACAGCTGTG AGAGACTC	1530
3' ARM of CRT; downstream of BLE with *BamH*I/*Not*I sites	GGGGGATCCATCGCCGAACAGAGTTGGTGG CTACGAG	GGTGGCGGCCGCGAGAGATTACCCTACTG CGCATCCGTAC	1440
P1/P2	GCGCCTTCGCAGCAGACTGATGTTCGAAG	GTGAGTCCGGAGCCTGAGAGGTCCTTC	1487
P3/P4	GAAGAGCAGATCGGGACCATTTTCGTC	CCCGTGCCTCCAGCGAAGCCTGTCTCTTC	1470
P5/P6	GCTCTGTAGGACTTGCATCACCAACGAG	GCGTGTCGCATACGAGCACCAGTACTAC	1647
P7/P8	CAGTTGTTTTAGTCGAACCGGTTAACA	GGAGCAGCGGATGCAAGCCTTTTTCTGTG	1542
Generation of CRT Complement (Fig. S2)			
P9/P14	CAGCACGTGACTCGATGTTTACCGCTGTC	CTCCGGCGTAGTCGGTGTACAAGGAG	4546
P11/P12	ATGGAGATGGCTGTCTAGTTAATTAATC	CCTGGCCGACGTGGATGCTGATAACCTC	2575
P13/14	CACAGACTGCTTGTGTACCTCCGTG	GTATGCACAGCACCGATGATGGCCATC	1490 (cDNA), 2837 (gDNA)
Generation of tdTomato-Atg8 (Fig. S2)			
5' Atg8 Int	CAG CAC GTG ACT CGA TGT TTA CCG CTG TC	CCA TGC GCA CCT TGA AGC GCA TGA ACT C	2842
3' Atg8 Int	CTA TCA GTTG TTT AGT CGA ACC GGT TAA C	CTG GCC GAC GTG GAT AAC CTC	2869
Parasite burden qPCR (Fig. 3)			
Tox9/11	AGG AGA GAT ATC AGG ACT GTA G	GCG TCG TCT CGT CTA GAT CG	
qPCR/Plaque assay (Fig. 2)			
α-**TUB**	GCG TCT TCT TGG ATT TGG AG	TGG AGA CCA GTG CAG TTG TC	

Figure S1

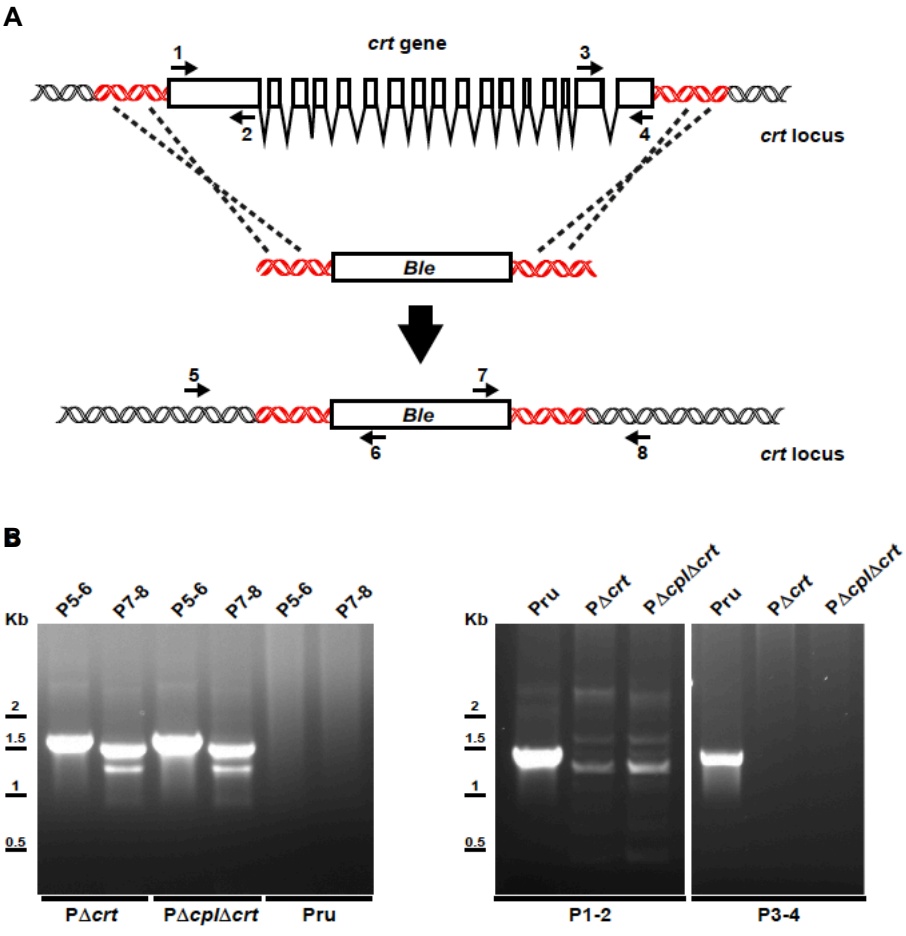
A
crt gene
1
2
3
4
crt locus
Ble
5
6
7
8
Ble
crt locus
B
Kb
P5-6
P7-8
P5-6
P7-8
P5-6
P7-8
2
1.5
1
0.5
PΔcrt
PΔcplΔcrt
Pru
Kb
Pru
PΔcrt
PΔcplΔcrt
Pru
PΔcrt
PΔcplΔcrt
2
1.5
1
0.5
P1-2
P3-4

Figure S2

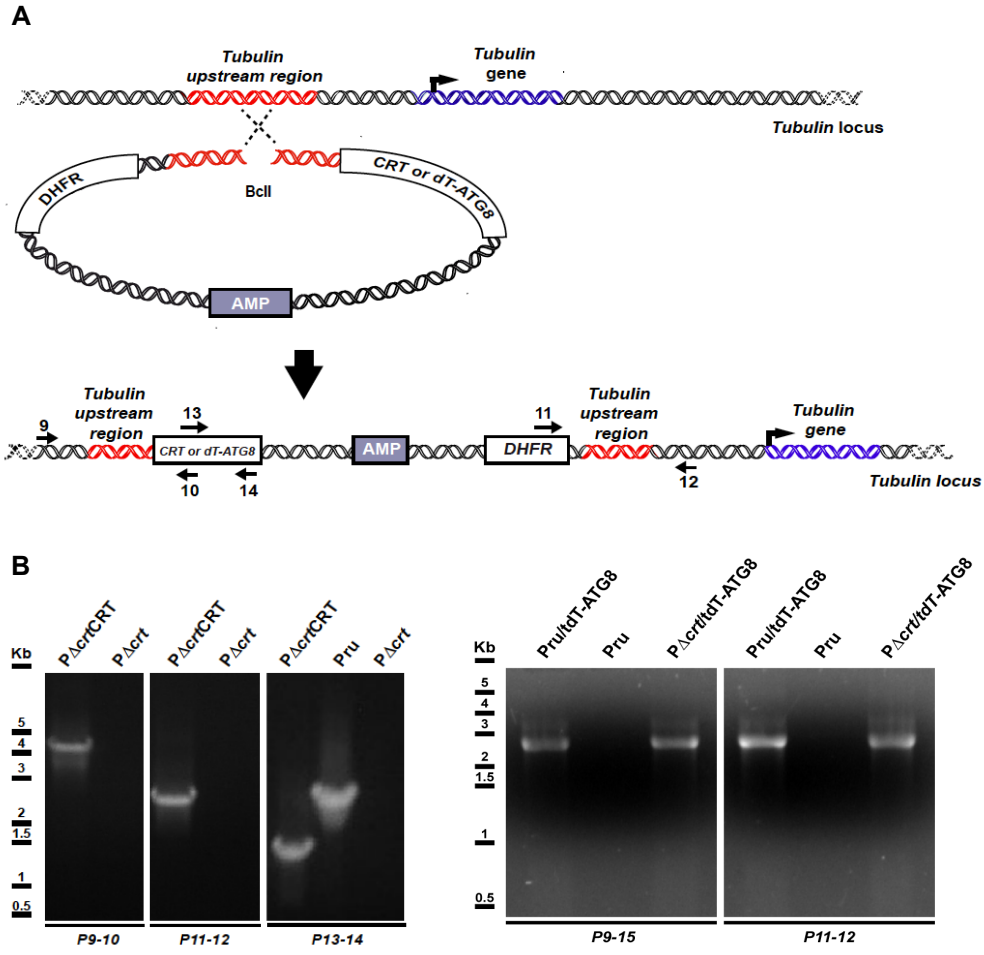
A
Tubulin upstream region
Tubulin gene
Tubulin locus
DHFR
BclI
CRT or dT-ATG8
AMP
Tubulin upstream region
9
13
CRT or dT-ATG8
AMP
DHFR
11
Tubulin upstream region
Tubulin gene
10
14
12
Tubulin locus
B
Kb
PΔcrtCRT
PΔcrt
PΔcrtCRT
PΔcrt
PΔcrtCRT
Pru
PΔcrt
5
4
3
2
1.5
1
0.5
P9-10
P11-12
P13-14
Kb
PrutdT-ATG8
Pru
PΔcrt/tdT-ATG8
PrutdT-ATG8
Pru
PΔcrt/tdT-ATG8
5
4
3
2
1.5
1
0.5
P9-15
P11-12

Figure S3

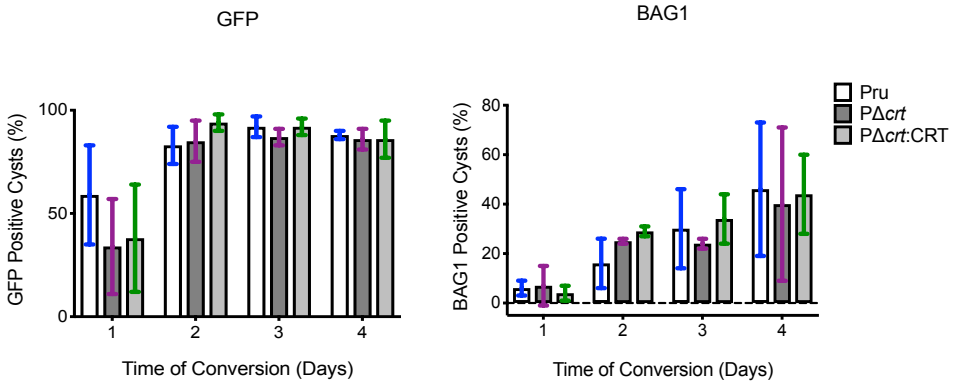
GFP
BAG1
GFP Positive Cysts (%)
BAG1 Positive Cysts (%)
100
50
0
80
60
40
20
0
1
2
3
4
Time of Conversion (Days)
Time of Conversion (Days)
Pru
PΔcrt
PΔcrt:CRT

Figure S4

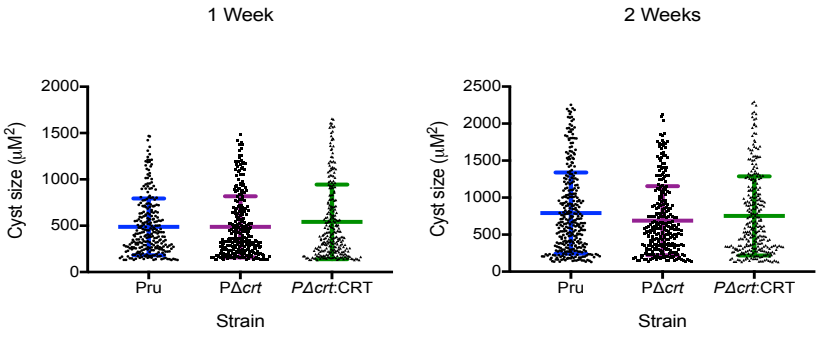
1 Week
2 Weeks
Cyst size (µM²)
2000
1500
1000
500
0
2500
Pru
PΔcrt
PΔcrt:CRT
Strain

Figure S5